

# Optimization design of GaAs-based betavoltaic batteries with p-n junction and Schottky barrier structures

Renzhou Zheng<sup>1</sup>, Jingbin Lu<sup>1\*</sup>, Xiaoyi Li<sup>1</sup>, Yu Wang<sup>1</sup>, Yumin Liu<sup>2</sup>, Xu Xu<sup>1</sup>, Ziyi Chen<sup>1</sup>, Xue Zhang<sup>1</sup>

<sup>1</sup> College of Physics, Jilin University, Changchun 130012, China

<sup>2</sup> College of Nuclear Science and Engineering, East China University of Technology, Nanchang 330013, China

This paper presents the calculation model and the optimization design of the GaAs-based betavoltaic batteries with p-n junction and Schottky barrier structures. First of all, by using the Monte Carlo code, the transport process and energy deposition distribution of the  $^{63}\text{Ni}$  source beta particles in the GaAs material are simulated. The relationships between the output parameters of the batteries and the physical parameters of the energy converter such as p-n junction depth, Schottky metal thickness, depletion region width and doping concentrations are discussed through the numerical calculation. For the GaAs p-n junction battery, the maximum output power density of  $0.135 \mu\text{W}/\text{cm}^2$  can be achieved when the junction depth is  $x_j=0.05 \mu\text{m}$ , the doping concentrations are  $N_a = 10^{18} \text{ cm}^{-3}$  and  $N_d = 2 \times 10^{15} \text{ cm}^{-3}$ . Meanwhile, the short-circuit current density, open-circuit voltage, filling factor and energy conversion efficiency are  $0.254 \mu\text{A}/\text{cm}^2$ ,  $0.638 \text{ V}$ ,  $83.3\%$  and  $2.63\%$ , respectively. Among the selected metals of Au, Pd, Ni and Pt for the GaAs Schottky barrier diodes, the Pt-GaAs battery has the best output performance due to its large work function. The maximum output power density of  $0.169 \mu\text{W}/\text{cm}^2$  can be achieved when a  $20 \text{ nm}$ -thick Schottky metal Pt is selected and the doping concentration is  $N_d = 10^{15} \text{ cm}^{-3}$ . The associated output parameters of the battery are  $0.234 \mu\text{A}/\text{cm}^2$ ,  $0.835 \text{ V}$ ,  $86.5\%$  and  $3.29\%$ , respectively.

Keywords: Betavoltaic battery, GaAs, p-n junction, Schottky barrier diode, Doping concentration

## 1. Introduction

With the development of Micro-Electro-Mechanical Systems (MEMS), the micro-scale energy systems have been increasingly studied for powering the micro-devices. A betavoltaic battery can be an appropriate option, due to its long service life, high power density, small scale, strong environmental adaptability and self-sufficient ability. In the past decade, researchers have done extensive studies on the betavoltaic batteries with p-n junction, p-i-n junction and Schottky barrier structures [1-3]. In these batteries, the beta particles interact with the semiconductor energy conversion material and the electron-hole pairs are generated. Then these electron-hole pairs can form the radiation-induced current through certain transport mechanisms. The electrical properties of semiconductors and the optimal design of device structure which directly affect the electron-hole pairs collection efficiency and the battery output performance, have become important theoretical research contents of a betavoltaic battery.

A betavoltaic battery generally consists of a beta isotope source and a semiconductor energy converter. Among beta-emitting isotope sources, most of them have beta energy that larger than  $300 \text{ keV}$ , and this energy is enough for a beta particle to displace a semiconductor atom in the energy converter. For a betavoltaic battery,

the semiconductor defect caused by atomic displacement can result in the performance degradation [1]. Several beta-emitting isotope sources have been investigated for the betavoltaic batteries, and the most appropriate three are  $^3\text{H}$ ,  $^{63}\text{Ni}$  and  $^{147}\text{Pm}$ , which meet the requirement of almost no radiation damage to most semiconductors. As for the semiconductor energy converter, theoretical studies have shown that the wider band gap can bring the higher energy conversion efficiency for a betavoltaic battery [4]. The wide band gap semiconductors are more attractive as the energy conversion materials than the narrow band gap semiconductors, due to their low leakage current and high radiation resistance. In recent years, GaAs, SiC, GaN and other wide band gap semiconductors have been successfully used in the betavoltaic batteries [5-12].

Compared with the traditional silicon material, GaAs as a direct band gap III-V compound semiconductor, has the advantages of wide band gap, strong heat stability, high electron mobility and high radiation resistance. Furthermore, the growth and processing techniques of GaAs are relatively mature and easier to implement than other wide band gap materials. It is easy to obtain the higher quality crystal samples. For these reasons, GaAs is widely used in the semiconductor industry, such as in optoelectronic devices and solar batteries [13]. The previous researches show that the GaAs material is suitable for the betavoltaic batteries based on the semiconductor devices such as the p-n junctions. When the self-absorption effect of the source is not considered, the maximum energy conversion efficiency of the GaAs-based betavoltaic batteries can reach to  $18.5\%$  [14]. However, the practically fabricated batteries do not show satisfactory output performance, and one of the reasons for this result

---

\*Supported by the National Natural Science Foundation of China (Nos. 11075064 and U1867210) and the National Major Scientific Instruments and Equipment Development Projects (No. 2012YQ240121). Corresponding author, Email address: ljb@jlu.edu.cn

is that the device design is not optimized enough. In 2011, a GaAs-<sup>63</sup>Ni betavoltaic battery with p-n junction structure was reported [15]. Their results show that in the depletion region only 20% of the electron-hole pairs are collected for the radiation-induced current. Under the irradiation of a 10 mCi/cm<sup>2</sup> <sup>63</sup>Ni source, the measured short-circuit current density is 18.16 nA/cm<sup>2</sup>. At the same year, they designed and fabricated a GaAs-based p<sup>+</sup>pn<sup>+</sup> junction battery, by optimizing the junction structure, the short-circuit current density of the battery has been increased to 28 nA/cm<sup>2</sup> [16]. In 2012, by using the Monte Carlo code MCNP, the transport process of the <sup>63</sup>Ni source beta particles in the GaAs material was simulated [17]. In this research, the source's self-absorption effect is considered, and the p-n junction depth, doping concentrations, electron-hole pairs collection efficiency, which affect the output performance of betavoltaic battery, were studied and analyzed. The physical parameters of the energy converter were optimized to achieve the higher energy conversion efficiency. Their theoretical calculations showed that the highest energy conversion efficiency of 4.34% can be achieved when the doping concentrations in p-type region and n-type region are  $N_a = 7.94 \times 10^{18} \text{ cm}^{-3}$  and  $N_d = 1.41 \times 10^{14} \text{ cm}^{-3}$  respectively. Until now, most of the theoretical research focused on the optimization design of the energy converter with p-n junction structure. However, the complex device structure and fabrication process of a p-n junction result in a poor reproducibility and high fabrication cost. A Schottky barrier diode seems to be the most effective way to fabricate a betavoltaic battery. In 2011, the electrical performance of a 4H-SiC Schottky barrier battery was predicted by a theoretical model [18]. And their experimental results also showed that this theoretical model was appropriate. In 2013, a theoretical analysis of the GaN Schottky barrier battery was presented [19]. Unfortunately, until this study, there has been little research on the theoretical model of a GaAs Schottky barrier battery. Therefore, it is necessary to have a theoretical analysis comparing the electrical properties of p-n junction battery and Schottky barrier battery based on the same semiconductor.

In this paper, we present a theoretical analysis of the main factors which affect the output performance of the GaAs p-n junction battery and the GaAs n-type doped/metal Schottky barrier battery. By using the Monte Carlo code, the transport process and energy deposition distribution of the <sup>63</sup>Ni source beta particles in the GaAs material are simulated. Then the relationships between the output parameters of the batteries and the physical parameters of the energy converter such as p-n junction depth, Schottky metal thickness, depletion region width and doping concentrations are established. Moreover, the doping concentrations are optimized to obtain the largest maximum output power density, and the corresponding output parameters are calculated. Finally, the output performance of the two types of batteries are compared to evaluate their application potential. These

results have guiding significance for the optimization and fabrication of the GaAs-based betavoltaic batteries with p-n junction and Schottky barrier structures.

## 2. Material and methods

### 2.1. Selection of source and semiconductor

Choosing a beta source need to consider its half-life, maximum decay energy, purity and power density, etc. Olsen recommended three beta-emitting isotope sources for the betavoltaic devices: <sup>3</sup>H, <sup>63</sup>Ni and <sup>147</sup>Pm [1]. The maximum beta energy of the <sup>3</sup>H source is 18.6 keV, which can reduce radiation damage to the semiconductor. However, due to its very low average beta energy (5.7 keV), the <sup>3</sup>H source is not suitable for a high-energy device. Although the <sup>147</sup>Pm source has a higher average beta energy (62 keV), it can produce a higher power density, it cannot be the best choice for a long-term application due to its shorter half-life (2.6 years). The beta spectrum of the <sup>63</sup>Ni source ( $E_{avg}=17.4 \text{ keV}$ ,  $E_{max}=66.9 \text{ keV}$ ) is relatively benign, it can provide sufficient power density and has a long half-life (100.1 years). In this study, <sup>63</sup>Ni is selected as the beta source of the betavoltaic battery.

For the semiconductor materials, three factors should be considered when selecting them: the radiation damage threshold energy, the electrical properties and the processing technology of material and devices. In this study, GaAs is selected as the semiconductor material for the betavoltaic batteries due to its high threshold energy for radiation damage (270 keV), wide band gap (1.424 eV) and high electron mobility ( $\sim 8000 \text{ cm}^2/(\text{V}\cdot\text{s})$ ) [3]. It also has low intrinsic carrier concentration, which contributes to the low leakage current and the high open-circuit voltage for a betavoltaic battery. The growth and processing techniques of GaAs are relatively mature, which is beneficial to fabricate a high quality betavoltaic device. Moreover, for the Schottky barrier battery, the metals of Au, Pd, Ni and Pt, which are often used to make Schottky contact with n-type doped GaAs, are selected. The parameters of GaAs material and metals are listed in Table 1 [20].

**Table 1**

The parameters of GaAs material and metals.

| Material | Parameter    | Value  |
|----------|--------------|--|
| GaAs     | $E_g$        | 1.424 eV                                     |
|          | $\chi$       | 4.07 eV                                      |
|          | $n_i$        | $2.25 \times 10^6 \text{ cm}^{-3}$           |
|          | $\epsilon_r$ | 13.1   |
|          | $N_c$        | $4.7 \times 10^{17} \text{ cm}^{-3}$         |
|          | $A^*$        | $8 \text{ A}/(\text{K}^2 \cdot \text{cm}^2)$ |
| Au       | $\phi_M$     | 5.1 eV                                       |
| Pd       |              | 5.12 eV                                      |
| Ni       |              | 5.15 eV                                      |
| Pt       |              | 5.65 eV                                      |

## 1 2 2.2. Structure design of the betavoltaic battery

### 3 2.2.1. p-n junction structure

4  
5 The operational principle of a betavoltaic battery with  
6 p-n junction structure is similar to that of a solar battery.  
7 When the beta particles enter into the GaAs material,  
8 they will lose their energy mainly through the ionizing  
9 radiation interactions. Meanwhile, in the GaAs material,  
10 electrons in the valence band are excited and jump to the  
11 conduction band, and the electron-hole pairs are formed.  
12 Then these electron-hole pairs are separated by the inter-  
13 nal electric field of the p-n junction and collected for the  
14 current. The schematic view of the betavoltaic battery  
15 with p-n junction structure is shown in Figure 1(a). In  
16 this figure,  $x_j$  is the junction depth,  $h$  is the thickness  
17 of n-type region.  $L_n$  is the minority electron diffusion  
18 length of p-type region and  $L_p$  is the minority hole diffu-  
19 sion length of n-type region. It should be mentioned that  
20 the p-type GaAs layer is selected as the emitting layer  
21 in the cell due to the larger electron diffusion length, it  
22 is beneficial to the collection of electron-hole pairs out-  
23 side the depletion region. The minority carrier diffusion  
lengths can be expressed as:

$$24 \quad 25 \quad 26 \quad 27 \quad 28 \quad 29 \quad 30 \quad 31 \quad 32 \quad 33 \quad 34 \quad L_{n,p} = \sqrt{D_{n,p}\tau_{n,p}} \quad (1)$$

35 where  $\tau$  is the minority carrier lifetime,  $D$  is the minority  
36 carrier diffusion coefficient, it can be calculated by the  
37 Einstein equation,  $D = \mu kT/q$ , where  $q$  is the electron  
38 charge,  $k$  is the Boltzmann's constant,  $T$  is the absolute  
39 temperature and  $\mu$  is the minority carrier mobility. For  
40 GaAs material (at 300 K), the minority electron mobility  
41  $\mu_n$  and the minority hole mobility  $\mu_p$  are related to the  
42 acceptor concentration  $N_a$  and the donor concentration  
43  $N_d$  respectively, they can be expressed as [21]:

$$44 \quad 45 \quad 46 \quad 47 \quad 48 \quad 49 \quad 50 \quad 51 \quad 52 \quad 53 \quad 54 \quad \mu_n = \frac{9400}{1 + (N_a/10^{17})^{0.5}} \text{ cm}^2/(\text{V}\cdot\text{s}) \quad (2)$$

$$55 \quad 56 \quad 57 \quad 58 \quad 59 \quad 60 \quad \mu_p = \frac{1}{2.5 \times 10^{-3} + 4 \times 10^{-21} \times N_d} \text{ cm}^2/(\text{V}\cdot\text{s}) \quad (3)$$

The minority electron lifetime and the minority hole lifetime can be expressed as [22]:

$$61 \quad 62 \quad 63 \quad 64 \quad 65 \quad \tau_n = \left( \frac{1.3 \times 10^9}{N_a} \right)^{0.9} \quad (4)$$

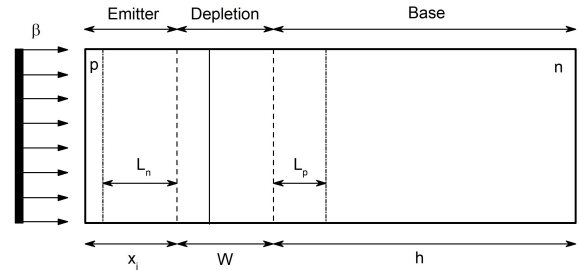
$$66 \quad 67 \quad 68 \quad 69 \quad 70 \quad \tau_p = \left( \frac{4 \times 10^9}{N_d} \right)^{0.92} \quad (5)$$

where  $\tau_n$  and  $\tau_p$  are in the units of s,  $N_a$  and  $N_d$  are in the units of  $\text{cm}^{-3}$ . Then the depletion region width  $W$  can be calculated by [23]:

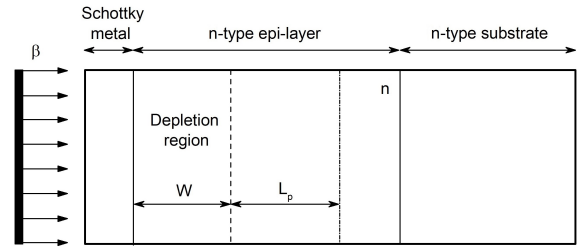
$$71 \quad 72 \quad 73 \quad 74 \quad 75 \quad W = \sqrt{V_{bi} \left( \frac{2\epsilon_r\epsilon_0}{q} \right) \left( \frac{N_a + N_d}{N_a N_d} \right)} \quad (6)$$

$$76 \quad 77 \quad 78 \quad 79 \quad 80 \quad V_{bi} = \frac{kT}{q} \left( \ln \frac{N_a N_d}{n_i^2} \right) \quad (7)$$

where  $\epsilon_r$  is the dielectric constant,  $\epsilon_0$  is the vacuum dielectric constant,  $V_{bi}$  is the built-in potential barrier and  $n_i$  is the intrinsic carrier concentration.



(a)



(b)

**Figure 1.** The schematic view of the betavoltaic batteries:  
(a) p-n junction structure and (b) Schottky barrier structure.

### 2.2.2. Schottky barrier structure

As shown in figure 1(b), the Schottky barrier battery mainly consists of a Schottky metal electrode, a n-type doped GaAs epilayer and a  $^{63}\text{Ni}$  source. The beta particles penetrate the Schottky metal and enter into the GaAs material, generating electron-hole pairs. Then these electron-hole pairs can be separated by the built-in potential and collected for the radiation-induced current. The depletion region width  $W$  can be calculated by [18, 19]:

$$W = \sqrt{\frac{2\epsilon_r\phi_i}{qN_d}} \quad (8)$$

where  $N_d$  is the donor concentration in n-type GaAs epilayer,  $\phi_i$  is the built-in potential and it can be calculated as follows:

$$\phi_i = \phi_B - \frac{kT}{q} \ln \left( \frac{N_c}{N_d} \right) \quad (9)$$

where  $\phi_B$  is the Schottky barrier height and  $N_c$  is the effective density of states in the conduction band of semiconductor. For a n-type semiconductor, the Schottky barrier height is obtained from:

$$\phi_B = \phi_M - \chi \quad (10)$$

where  $\chi$  is the electron affinity potential of the semiconductor and  $\phi_M$  is the work function of the Schottky metal.

### 2.3. Simulation of the energy deposition distribution

The electrical energy of a betavoltaic battery is derived from the energy deposition of beta particles in the semiconductor energy converter caused by the ionizing radiation interactions. The energy deposition distribution of the beta particles in the energy converter determines the number and position of electron-hole pairs, which further affect the output performance of the battery. Therefore, the transport process of the beta particles in the semiconductor energy conversion material is an important research content in the calculation and analysis of battery performance. In this part, by using the Monte Carlo code, the energy deposition distribution of the  $^{63}\text{Ni}$  source beta particles in the GaAs material are simulated. Different from the p-n junction battery, for the Schottky barrier battery, the beta particles penetrate the Schottky metal layer (Au, Pd, Ni or Pt) first, and then enter into the GaAs material. Therefore, the energy deposition loss and the reflection loss in the Schottky metal should be considered. The prototype structure of the simulation model is shown in figure 2. The full energy spectrum of  $^{63}\text{Ni}$  source is used to calculate the energy deposition along the radiation transport depth in GaAs bulk ( $1\text{ cm} \times 1\text{ cm} \times 0.5\text{ cm}$ ). Various thicknesses of  $^{63}\text{Ni}$  source ( $1\text{ cm} \times 1\text{ cm} \times H$ ) are used to obtain the optimal thickness of source. For the Schottky barrier battery, the part of GaAs material ( $1\text{ cm} \times 1\text{ cm} \times h$ ) between the  $^{63}\text{Ni}$  source and the energy converter is replaced with the Schottky metal (Au, Pd, Ni or Pt).

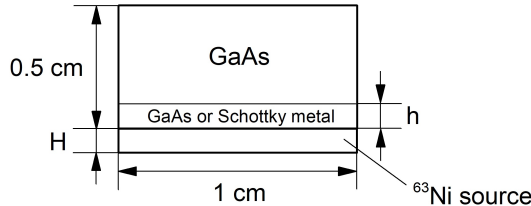


**Figure 2.** The prototype structure of the simulation model.

For the rectangular  $^{63}\text{Ni}$  sources with various thicknesses, the total energy deposition power density in GaAs material increases with the thickness of source increasing. When the source thickness is more than  $2\text{ }\mu\text{m}$ , due to the self-absorption effect of source, the total energy deposition power density increases slowly and then tends to the saturation value. If the source thickness continues to increase, it will not bring larger apparent power density, but lower utilization efficiency of source. Therefore, a  $2\text{ }\mu\text{m}$ -thick  $^{63}\text{Ni}$  source (total activity density of  $100\text{ mCi/cm}^2$ ) is selected for the GaAs-based batteries. The relationship between the energy deposition rate in the GaAs material and the radiation transport depth is shown in figure 3, which shows that the energy deposition rate in the material decreases exponentially with the increasing of the radiation transport depth. It can be

expressed by the formula:  $dE/dX = G_0 e^{-\alpha X}$ , where  $X$  is the radiation transport depth,  $G_0$  is the energy deposition rate on the surface of the material and  $\alpha$  is the absorption coefficient, respectively. Moreover, for the Schottky barrier batteries, the type and thickness ( $h$ ) of the Schottky metal affect the energy deposition distribution in semiconductor. Especially, the fitting parameters (with  $20\text{ nm}$ -thick metal) and the energy backscattering coefficient are listed in Table 2. Here, the energy backscattering coefficient is defined as the energy of backscattering beta particles divided by the energy of incident beta particles entering into the energy converter (GaAs or Schottky metal).

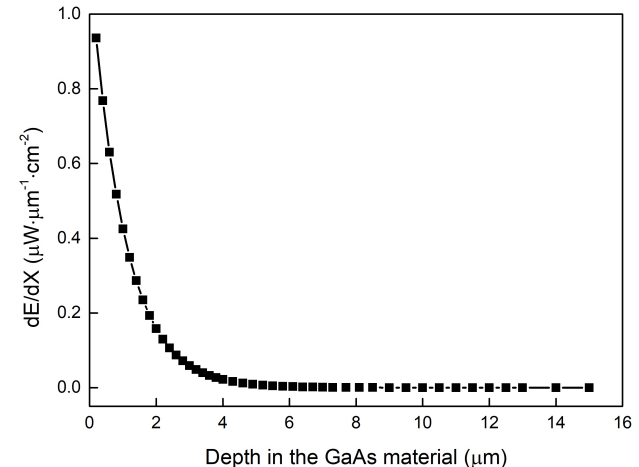


**Figure 3.** The energy deposition rate in the GaAs material versus the radiation transport depth.

**Table 2**

The fitting parameters (with  $20\text{ nm}$ -thick metal) and the energy backscattering coefficient.

| Target materials | $G_0(\mu\text{W}\cdot\mu\text{m}^{-1}\cdot\text{cm}^2)$ | $\alpha(\mu\text{m}^{-1})$ | Energy backscattering coefficient (%) |
|------------------|---|----------------------------|---------------------------------------|
| GaAs             | 1.14062   | 0.98767                    | 36.3                                  |
| Au-GaAs          | 1.04010   | 0.98045                    | 38.7                                  |
| Pd-GaAs          | 1.05557   | 0.96649                    | 36.8                                  |
| Ni-GaAs          | 1.08663   | 0.97970                    | 35.9                                  |
| Pt-GaAs          | 1.02983   | 0.97958                    | 38.9                                  |

The relationship between the total energy deposition power density in the GaAs material and the thickness of metal is shown in figure 4. When the thickness of metal increases from  $20\text{ nm}$  to  $200\text{ nm}$ , the total energy deposition power densities of the beta particles in the GaAs material decrease in different degrees. For the GaAs covered with metal Pt, due to the high atomic number and mass density of Pt, the total energy deposition power density drops the most. Moreover, as shown in Table 2, the metal Ni has smaller energy backscattering coefficient, and the Ni-GaAs Schottky barrier batteries will have more electron-hole pairs produced due to larger total energy deposition power density in GaAs (covered

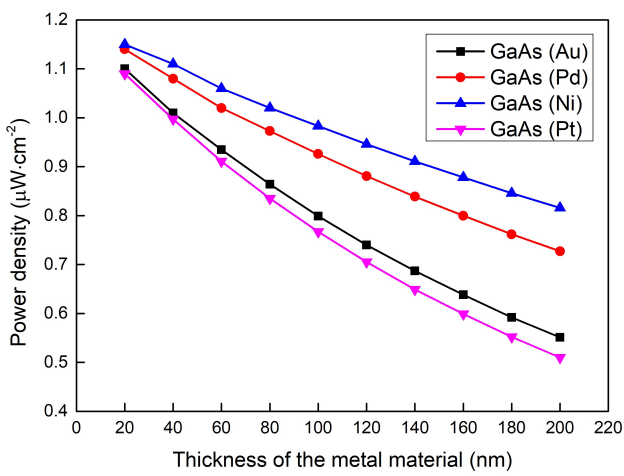


**Figure 4.** The total energy deposition power density in the GaAs material versus the thickness of metal materials.

with metal Ni). In addition, it is worth noting that the energy backscattering coefficient of metal Ni is smaller than that of GaAs, because the atomic number of Ni ( $Z=28$ ) is lower than that of GaAs ( $Z=32$ ). However, due to the absorption loss in metal Ni, the total energy deposition power density in GaAs ( $1.152 \mu\text{W}/\text{cm}^2$ ) which is covered with metal Ni, is still smaller than that in un-covered GaAs material ( $1.204 \mu\text{W}/\text{cm}^2$ ).

### 3. Performance calculation model

#### 3.1. The calculation of short-circuit current density

In the semiconductor energy converter, the generation rate of electron-hole pairs is related to the energy deposition rate ( $dE/dX$ ) of the beta particles and the mean ionization energy ( $E_{ehp}$ ) of the semiconductor material. Klein gave the average energy dissipated per electron-hole pair generated as  $E_{ehp} = 2.8E_g + 0.5 \text{ eV}$ , where  $E_g$  is the band gap of the semiconductor [24]. The electron-hole pairs collection efficiency is determined by the junction depth (for p-n junction) and other structural parameters of the junction. Electron-hole pairs generated in the depletion region are considered to be collected with 100% efficiency, while the collection efficiency of electron-hole pairs outside the depletion region depends on the distance to the depletion region and the minority carrier diffusion length. And the radiation-induced current density (short-circuit current density) can be calculated by solving the electron/hole continuity equation and ambipolar transport equation in different regions.

##### 3.1.1. p-n junction-based cell

According to figure 1(a), the radiation-induced current densities ( $J_{sc}$ ) in the emitter layer ( $J_E$ ), the base layer ( $J_B$ ) and the depletion region ( $J_D$ ) are expressed as [25-

27]:

$$J_E = \frac{G_0 L_n}{\alpha^2 L_n^2 - 1} \times \frac{q}{E_{ehp}} \times \left\{ \frac{\frac{S_n L_n}{D_n} + \alpha L_n - \exp(-\alpha x_j) \left[ \frac{S_n L_n}{D_n} \cosh\left(\frac{x_j}{L_n}\right) + \sinh\left(\frac{x_j}{L_n}\right) \right]}{\frac{S_n L_n}{D_n} \sinh\left(\frac{x_j}{L_n}\right) + \cosh\left(\frac{x_j}{L_n}\right)} - \alpha L_n \exp(-\alpha x_j) \right\} \quad (11)$$

$$J_B = \frac{G_0 L_p}{\alpha^2 L_p^2 - 1} \exp[-\alpha(x_j + W)] \times \frac{q}{E_{ehp}} \times \left\{ \alpha L_p - \frac{\frac{S_p L_p}{D_p} \left[ \cosh\left(\frac{h}{L_p}\right) - \exp(-\alpha h) \right] + \sinh\left(\frac{h}{L_p}\right) + \alpha L_p \exp(-\alpha h)}{\frac{S_p L_p}{D_p} \sinh\left(\frac{h}{L_p}\right) + \cosh\left(\frac{h}{L_p}\right)} \right\} \quad (12)$$

$$J_D = \frac{G_0}{\alpha} e^{-\alpha x_j} (1 - e^{-\alpha W}) \times \frac{q}{E_{ehp}} \quad (13)$$

where  $S$  is the surface recombination velocity of the carriers. Then, the short-circuit current density ( $J_{sc}$ ) is expressed as:

$$J_{sc} = J_E + J_B + J_D \quad (14)$$

because the energy deposition rate in the target material decreases exponentially with the increasing of the radiation transport depth, the p-n junction with a depletion region close to the device surface, in other words, has a shallow junction depth, can collect more electron-hole pairs. Referring to the mature processing techniques of shallow junction in most of researches, the minimum junction depth ( $x_j$ ) of  $0.05 \mu\text{m}$  is selected for the calculation model in this work.

##### 3.1.2. Schottky barrier-based cell

According to figure 1(b), the short-circuit current density ( $J_{sc}$ ) consists of the depletion region current density ( $J_D$ ) and the neutral region current density ( $J_N$ ), it can be calculated by [19]:

$$J_{sc} = J_D + J_N = \frac{q}{E_{ehp}} \left[ \int_0^W \frac{dE}{dX} dX + \int_W^{W+L_p} \frac{dE}{dX} e^{\frac{W-X}{L_p}} dX \right] \quad (15)$$

where  $dE/dX$  is the energy deposition rate in the semiconductor material, which is a function of the radiation transport depth  $X$  (see Table 2). Different from the previous studies which introduced a metal penetration coefficient (ranging from 0 to 1) to consider the absorption loss of Schottky metal [18, 19], the energy deposition distribution of beta particles in the semiconductor material

1  
2  
3  
4  
5  
6  
7  
8  
9  
10  
11  
12  
13  
14  
15  
16  
17  
18  
19  
20  
21  
22  
23  
24  
25  
26  
27  
28  
29  
30  
31  
32  
33  
34  
35  
36  
37  
38  
39  
40  
41  
42  
43  
44  
45  
46  
47  
48  
49  
50  
51  
52  
53  
54  
55  
56  
57  
58  
59  
60  
after penetrating the Schottky metal is simulated in this study. Only the energy deposition rate in GaAs is fitted with exponential function, and then the generation rate of electron-hole pair is calculated.

### 3.2. Leakage current density and open-circuit voltage

The open-circuit voltage is related to the short-circuit current density and the leakage current density. For a p-n junction, the leakage current density ( $J_0$ ) is expressed as follows [28]:

$$J_0 = q \frac{n_i^2}{N_a} \frac{D_n}{L_n} \left[ \frac{\frac{D_n}{L_n} \sinh\left(\frac{x_j}{L_n}\right) + S_n \cosh\left(\frac{x_j}{L_n}\right)}{\frac{D_n}{L_n} \cosh\left(\frac{x_j}{L_n}\right) + S_n \sinh\left(\frac{x_j}{L_n}\right)} \right] + q \frac{n_i^2}{N_d} \frac{D_p}{L_p} \left[ \frac{\frac{D_p}{L_p} \sinh\left(\frac{h}{L_p}\right) + S_p \cosh\left(\frac{h}{L_p}\right)}{\frac{D_p}{L_p} \cosh\left(\frac{h}{L_p}\right) + S_p \sinh\left(\frac{h}{L_p}\right)} \right] \quad (16)$$

For a Schottky barrier diode, the leakage current density ( $J_0$ ) is expressed as [18]:

$$J_0 = A^* T^2 \exp\left(-\frac{q\phi_B}{kT}\right) \quad (17)$$

where  $A^*$  is the effective Richardson constant of thermal electron emission, which is equal to  $8 \text{ A}/(\text{K}^2 \cdot \text{cm}^2)$  for n-type GaAs.

For a betavoltaic battery with p-n junction or Schottky barrier structure, the open-circuit voltage ( $V_{oc}$ ) is obtained from:

$$V_{oc} = \frac{nkT}{q} \ln\left(\frac{J_{sc}}{J_0} + 1\right) \quad (18)$$

where  $n$  is an ideal factor.

### 3.3. Output power density and energy conversion efficiency

Generally, the maximum output power density and the energy conversion efficiency are used to evaluate the output performance of a betavoltaic battery. The maximum output power density ( $P_m$ ) as a function of  $V_{oc}$ ,  $J_{sc}$  and filling factor ( $FF$ ) is expressed as follows [29]:

$$P_m = FF \times V_{oc} \times J_{sc} \quad (19)$$

$$FF = \frac{\frac{q}{kT} V_{oc} - \ln\left(\frac{q}{kT} V_{oc} + 0.72\right)}{\frac{q}{kT} V_{oc} + 1} \quad (20)$$

The energy conversion efficiency ( $\eta$ ) refers to the ratio of the maximum output power density ( $P_m$ ) to the total power density ( $P_{total}$ ) produced in the source, it can be expressed as:

$$\eta = \frac{P_m}{P_{total}} \quad (21)$$

In our simulation model, the GaAs energy converter is placed on the surface of the source, but for a practical fabricated battery, two cells are placed on both sides of the source to optimize the efficiency. Therefore, the energy conversion efficiency of the GaAs-based battery is calculated by using the maximum output power density for a single side of the cell and multiplying by 2.

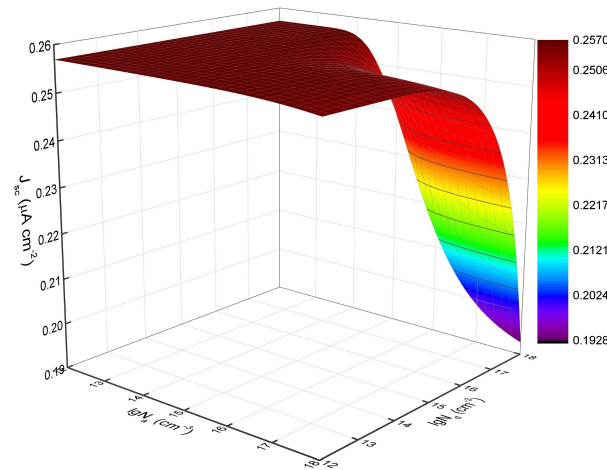
## 4. Results and discussion

### 4.1. The output performance of a GaAs p-n junction-based battery

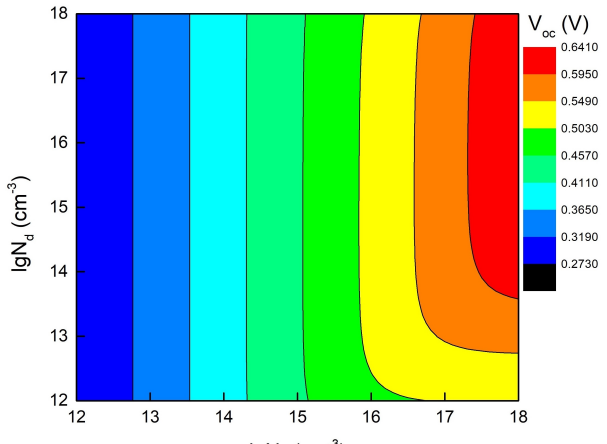
For the GaAs p-n junction-based battery in this work, the minimum junction depth is  $0.05 \mu\text{m}$ . As presented in figure 5(a), the short-circuit current density increases with the decreasing of doping concentrations ( $N_a$  and  $N_d$ ). In general, the low doping concentrations bring a wide depletion region and a long minority carrier diffusion length, which contribute to improving the collection efficiency of the radiation-induced electron-hole pairs within the energy deposition region of  $5.8 \mu\text{m}$ . When  $N_a$  is less than  $10^{14} \text{ cm}^{-3}$  or  $N_d$  is less than  $10^{16} \text{ cm}^{-3}$ , the short-circuit current density tend to a saturation value of  $0.257 \mu\text{A}/\text{cm}^2$ .

Then, according to Eq. (18), the open-circuit voltage is determined by  $J_{sc}$  and  $J_0$ . Furthermore,  $J_{sc}$  decreases with the increasing of doping concentrations ( $N_a$  and  $N_d$ ). While based on Eq. (16),  $J_0$  decreases rapidly by several orders of magnitude as  $N_a$  increases. To be specific, when  $N_a$  increases from  $10^{12} \text{ cm}^{-3}$  to  $10^{18} \text{ cm}^{-3}$ ,  $J_0$  decreases from  $6.716 \times 10^{-6} \mu\text{A}/\text{cm}^2$  ( $N_d = 10^{12} \text{ cm}^{-3}$ ) to  $8.439 \times 10^{-10} \mu\text{A}/\text{cm}^2$  ( $N_d = 10^{12} \text{ cm}^{-3}$ ). While  $N_d$  increases from  $10^{12} \text{ cm}^{-3}$  to  $10^{18} \text{ cm}^{-3}$ ,  $J_0$  only decreases from  $8.439 \times 10^{-10} \mu\text{A}/\text{cm}^2$  ( $N_a = 10^{18} \text{ cm}^{-3}$ ) to  $4.379 \times 10^{-12} \mu\text{A}/\text{cm}^2$  ( $N_a = 10^{18} \text{ cm}^{-3}$ ), it is more sensitive to  $N_a$ . Therefore, as shown in figure 5(b), the peak  $V_{oc}$  of  $0.641 \text{ V}$  appears when the p-type region is heavily doped ( $N_a \approx 10^{18} \text{ cm}^{-3}$ ).

Figure 6(a) shows the result for the maximum output power density versus the doping concentrations ( $N_a$  and  $N_d$ , with  $0.05 \mu\text{m}$ -junction depth). It can be seen that a p-type doped region with heavy doping is beneficial to achieve the larger maximum output power density. In the non-degenerate case for GaAs, the doping concentrations should be no more than  $10^{18} \text{ cm}^{-3}$ , the largest maximum output power density of  $0.135 \mu\text{W}/\text{cm}^2$  can be obtained when the doping concentrations are  $N_a = 10^{18} \text{ cm}^{-3}$  and  $N_d = 2 \times 10^{15} \text{ cm}^{-3}$ . And the related values of  $J_{sc}$ ,  $V_{oc}$ ,  $FF$  and  $\eta$  are  $0.254 \mu\text{A}/\text{cm}^2$ ,  $0.638 \text{ V}$ ,  $83.3\%$  and  $2.63\%$ , respectively. It should be mentioned that the junction depth of the GaAs energy converter affect the maximum output power density of the p-n junction battery due to the change in the location of the electron-hole pairs collection region. Then the optimal doping concentrations ( $N_a$  and  $N_d$ ) are different for various GaAs p-n junction-based batteries. Furthermore, in figure 6(b), the relation-



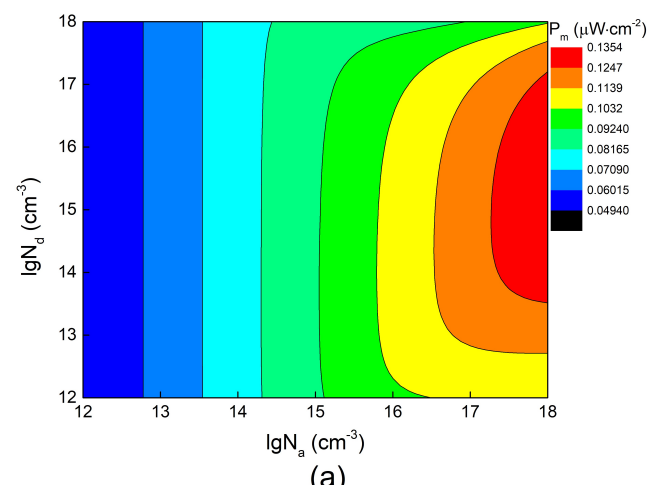
(a)



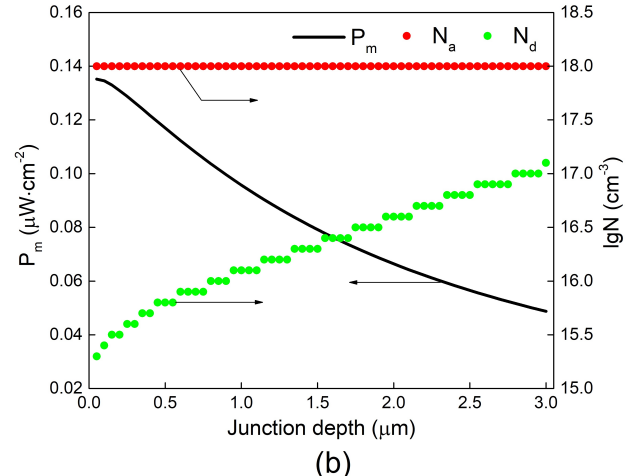
(b)

**Figure 5.** The (a) short-circuit current density and (b) open-circuit voltage of the GaAs p-n junction battery versus the doping concentrations ( $N_a$  and  $N_d$ , with 0.05  $\mu\text{m}$ -junction depth).

ship among the maximum output power density, the optimal doping concentrations ( $N_a$  and  $N_d$ ) and the junction depth is obtained. As the junction depth becomes shallow, the depletion region is getting closer and closer to where the beta particles enter, and the generation rate of electron-hole pairs is higher in this position. Ultimately, the shallower junction is benefit to the larger maximum output power density of a p-n junction betavoltaic battery. To be specific, when the junction depth decreases from 3  $\mu\text{m}$  to 0.05  $\mu\text{m}$ , the maximum output power density of the battery increases from 0.049  $\mu\text{W}/\text{cm}^2$  to 0.135  $\mu\text{W}/\text{cm}^2$ . Therefore, the junction depth should be reduced as much as possible for a p-n junction betavoltaic battery. The results of calculation also show that when the junction depth increases,  $J_{sc}$  decreases and becomes more sensitive to  $N_a$  than  $N_d$ , meanwhile,  $J_0$  also decreases and decreases greatly when the p-type region and



(a)



(b)

**Figure 6.** (a) The maximum output power density of the GaAs p-n junction battery versus the doping concentrations ( $N_a$  and  $N_d$ , with 0.05  $\mu\text{m}$ -junction depth). (b) The maximum output power density, optimal doping concentrations ( $N_a$  and  $N_d$ ) versus the junction depth.

n-type region are heavily doped ( $\sim 10^{18} \text{ cm}^{-3}$ ). As a result, when the p-type region is heavily doped and n-type region is lightly doped,  $V_{oc}$  of a shallow junction battery is larger than that of a deep junction battery. Conversely, when the p-type region and n-type region are both heavily doped,  $V_{oc}$  of a shallow junction battery is smaller than that of a deep junction battery. The doping concentration  $N_d$  which can make  $V_{oc}$  reach to its maximum value will increase as the junction depth increases. That is why when the junction depth increases from 0.05  $\mu\text{m}$  to 3  $\mu\text{m}$ , the optimal doping concentration  $N_d$  increases from  $2 \times 10^{15} \text{ cm}^{-3}$  to  $1.26 \times 10^{17} \text{ cm}^{-3}$ . Besides, the optimal doping concentration  $N_a$  is always  $10^{18} \text{ cm}^{-3}$  due to the limit of doping concentrations in non-degenerate GaAs.

## 4.2. The output performance of a GaAs Schottky barrier-based battery

In figure 7(a), for the Au-GaAs Schottky barrier-based batteries with some specific Schottky metal thicknesses, the relationship between the short-circuit current density and the doping concentration ( $N_d$ ) is shown. It is seen that the short-circuit current density decreases very slowly and then sharply with the increasing of  $N_d$ . Then, when the doping concentration  $N_d$  is less than  $10^{15} \text{ cm}^{-3}$ , the short-circuit current density tends to a saturation value. The main reason is that both the depletion region and minority carrier diffusion region are wide enough to collect almost all the radiation-induced electron-hole pairs with the low doping concentration ( $N_d$ ). Furthermore, due to the absorption effect of Schottky metal to the beta particles, if  $N_d$  is selected, the thinner Au layer contributes to the higher short-circuit current density of a battery. Then, as presented in figure 8(a), in the calculation model, the metals of Au, Pd, Ni and Pt are selected. When the doping concentration  $N_d$  is  $10^{15} \text{ cm}^{-3}$  in the GaAs region, the relationship between the short-circuit current density and the thickness of metals is obtained. It can be seen that due to the stronger absorption effect of metal Pt to the beta particles, the Pt-GaAs Schottky barrier batteries have lower short-circuit current density. When the thickness of Schottky metals increases from 20 nm to 200 nm, the short-circuit current density of the Pt-GaAs Schottky barrier batteries decreases rapidly. The Ni-GaAs Schottky barrier batteries show better performance in terms of the short-circuit current density.

In figure 7(b), for the GaAs Schottky barrier-based batteries with Au, the result for the open-circuit voltage versus the doping concentration ( $N_d$ ) is shown. When  $N_d$  is less than  $10^{15} \text{ cm}^{-3}$ , the open-circuit voltage almost remains unchanged, which is similar to the short-circuit current density. According to Eq. (17) and (18), the dependence of  $V_{oc}$  on  $N_d$  mainly lies in the influence of  $N_d$  on  $J_{sc}$ . Next, as presented in figure 8(b), for the batteries with Au, Pd, Ni and Pt, when the doping concentration  $N_d$  is  $10^{15} \text{ cm}^{-3}$ , the result for the open-circuit voltage versus the thickness of metals is obtained. Obviously, the open-circuit voltage depends strongly on the work function of Schottky metal. Although the Pt-GaAs Schottky barrier batteries have the smaller short-circuit current density, due to the larger work function of metal Pt, the higher Schottky barrier height and lower leakage current density can be obtained, so they have the higher open-circuit voltage. Taking a battery with the metal Pt of 20 nm as example, the maximum open-circuit voltage of the Pt-GaAs Schottky barrier battery can reach to 0.835 V. As the thickness of Schottky metal materials increases, the open-circuit voltage of the GaAs Schottky barrier batteries decreases slightly.

The results in figure 7(c) show the relationship between the maximum output power density of the Au-GaAs Schottky barrier batteries and the doping concentration ( $N_d$ ). It can be seen that the variation

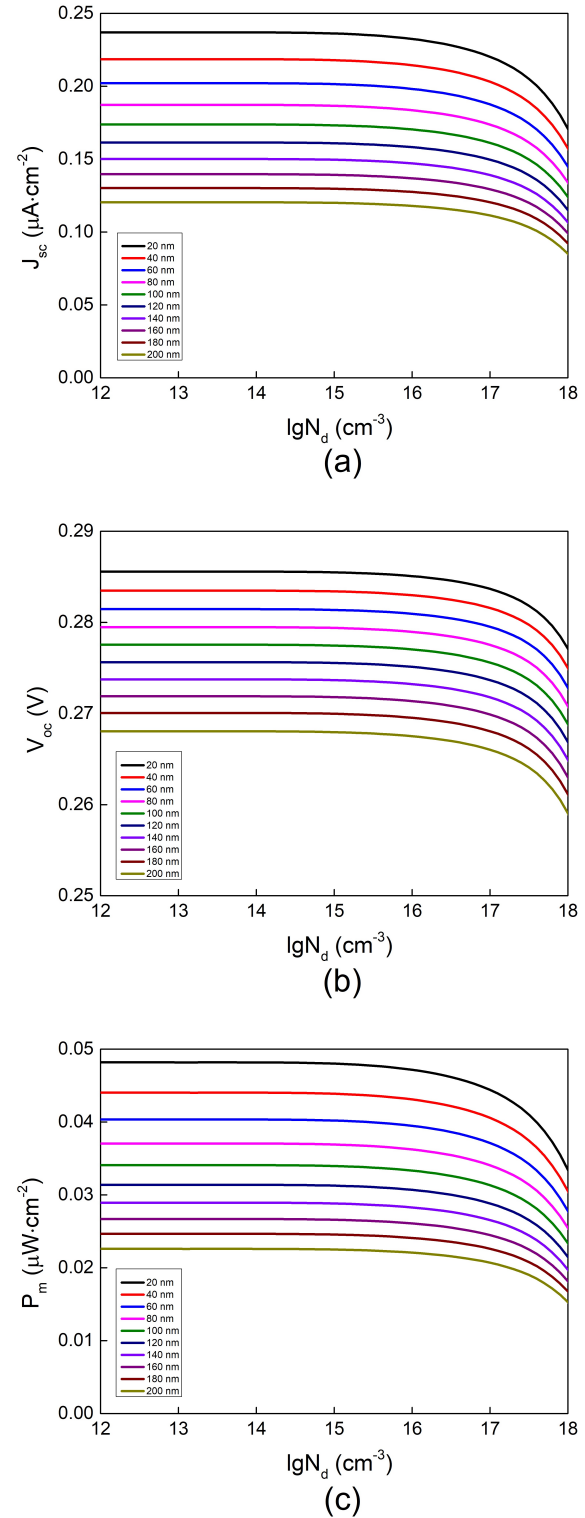


**Figure 7.** The (a) short-circuit current density, (b) open-circuit voltage and (c) maximum output power density of the Au-GaAs Schottky barrier batteries versus the doping concentration ( $N_d$ ).

trend of the maximum output power density is similar to that of the short-circuit current density. The

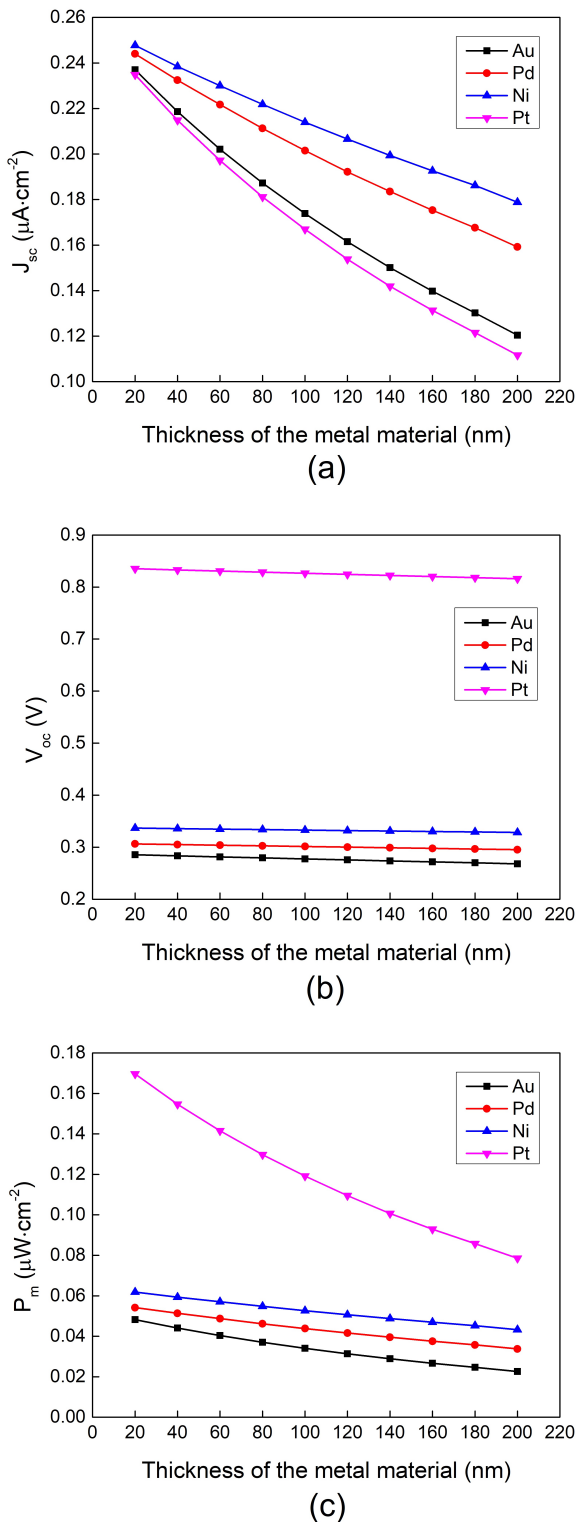


**Figure 8.** The (a) short-circuit current density, (b) open-circuit voltage and (c) maximum output power density of the GaAs Schottky barrier batteries ( $N_d = 10^{15} \text{ cm}^{-3}$ ) versus the thickness of metal materials.

largest maximum output power density can be achieved when the collection region and generation region of

the radiation-induced electron-hole pairs are highly matched. When the doping concentration  $N_d$  increases from  $10^{17} \text{ cm}^{-3}$  to  $10^{18} \text{ cm}^{-3}$ , the depletion region width  $W$  decreases from  $0.12 \mu\text{m}$  to  $0.04 \mu\text{m}$ , and the minority hole diffusion length  $L_p$  decreases from  $11.81 \mu\text{m}$  to  $2.74 \mu\text{m}$ , which is smaller than the range of energy deposition ( $5.8 \mu\text{m}$ ). As a result, the maximum output power density decreases rapidly when  $N_d$  is larger than  $10^{17} \text{ cm}^{-3}$ . In figure 8(c), for the batteries with Au, Pd, Ni and Pt, when the doping concentration  $N_d$  is  $10^{15} \text{ cm}^{-3}$ , the result for the maximum output power density versus the thickness of metals is obtained. For an example, the GaAs n-type/metal Schottky barrier cell, which is designed with the metal of larger work function, higher Schottky barrier height and lower leakage current density, can achieve the better performance. Obviously, this factor has a greater influence on the maximum output power density than the effect of the absorption of beta particles by the Schottky metal in this work. Moreover, for the Pt-GaAs Schottky barrier batteries, the thickness of Schottky metals has a greater effect on the short-circuit current density. As a result, when the thickness of metal layer increases, the maximum output power density attenuation is more significant than that of other batteries. The comparison of optimized output performances of the GaAs-based batteries is shown in Table 3.

**Table 3**

The comparison of optimized output performances of the GaAs-based batteries.

| Battery type | $J_{sc}$<br>( $\mu\text{A}/\text{cm}^2$ ) | $V_{oc}$ (V) | $P_m$<br>( $\mu\text{W}/\text{cm}^2$ ) | FF(%) | $\eta$ (%) |
|--------------|---|--------------|--|-------|------------|
| p-n junction | 0.254                                     | 0.638        | 0.135                                  | 83.3  | 2.63       |
| Au-GaAs      | 0.236                                     | 0.285        | 0.048                                  | 71.4  | 0.93       |
| Pd-GaAs      | 0.243                                     | 0.306        | 0.054                                  | 72.6  | 1.05       |
| Ni-GaAs      | 0.247                                     | 0.337        | 0.062                                  | 74.5  | 1.20       |
| Pt-GaAs      | 0.234                                     | 0.835        | 0.169                                  | 86.5  | 3.29       |

It is seen that due to the absorption loss of beta particles in Schottky metals, the Schottky barrier batteries with Au, Pd, Ni and Pt, have less electron-hole pairs produced than the p-n junction battery, further resulting in the smaller short-circuit current density. For the Schottky barrier batteries with Au, Pd and Ni, which have the small work function, their open-circuit voltage and maximum output power density are also lower than that of the p-n junction battery. And as the thickness of metals increases, these output parameters will be even lower. In contrast, due to the very large work function of metal Pt, the Pt-GaAs Schottky barrier diode have a higher Schottky barrier height, and this battery can have a lower leakage current density. As a result, the Pt-GaAs Schottky barrier-based battery has the higher open-circuit voltage and maximum output power density than the GaAs p-n junction-based battery.

## 1 2 3 4 5 6 7 8 9 10 11 12 13 14 15 16 17 18 19 20 21 22 23 24 25 26 27 28 29 30 31 32 33 34 35 36 37 38 39 40 41 42 43 44 45 46 47 48 49 50 51 52 53 54 55 56 57 58 59 60 5. Conclusion

In summary, in the means of the simulation and the numerical calculation, the performance calculation model on the GaAs- $^{63}\text{Ni}$  batteries with the p-n junction and the GaAs n-type doped/metal Schottky barrier diode are built. For the batteries with the Schottky barrier diode, the metals of Au, Pd, Ni and Pt are selected. The transport process and the energy deposition distribution of the  $^{63}\text{Ni}$  source beta particles in the GaAs material are simulated. For a GaAs p-n junction-based battery, the influence of the junction depth and the doping concentrations ( $N_a$  and  $N_d$ ) on the output performance is investigated. When the junction depth  $x_j$  of  $0.05\ \mu\text{m}$ , the doping concentrations  $N_a$  of  $10^{18}\ \text{cm}^{-3}$  and  $N_d$  of  $2 \times 10^{15}\ \text{cm}^{-3}$  are set, the maximum output power density of  $0.135\ \mu\text{W}/\text{cm}^2$  can be obtained. And the related  $J_{sc}$ ,  $V_{oc}$ , FF and  $\eta$  are  $0.254\ \mu\text{A}/\text{cm}^2$ ,  $0.638\ \text{V}$ , 83.3% and 2.63%, respectively. For a GaAs Schottky barrier-based battery, the Schottky metal with a larger work function contributes to the higher Schottky barrier height and then results in the better output performance. Among the metals of Au, Pd, Ni and Pt, the output performance of the Pt-GaAs Schottky barrier battery is the best and that of the Au-GaAs Schottky barrier battery is the worst under the same structure and radiation source. Taking the Pt-GaAs Schottky barrier battery as an example, when a 20 nm-thick Schottky metal Pt is selected and the doping concentration  $N_d$  is  $10^{15}\ \text{cm}^{-3}$ , the maximum output power density of  $0.169\ \mu\text{W}/\text{cm}^2$  can be obtained. And the related  $J_{sc}$ ,  $V_{oc}$ , FF and  $\eta$  are  $0.234\ \mu\text{A}/\text{cm}^2$ ,  $0.835\ \text{V}$ , 86.5% and 3.29%, respectively. Finally, the calculation results show that the betavoltaic battery based on a Pt-GaAs (n-type doped) Schottky barrier diode has the better performance than a GaAs p-n junction, due to the lower leakage current density. These results indicate that the Schottky barrier diode could be a potential candidate for energy converter of the betavoltaic battery.

## 40 Acknowledgements

41 This work was supported by the National Natural Science Foundation of China (Nos. 11075064 and U1867210)  
42 and the National Major Scientific Instruments and Equipment Development Projects (No. 2012YQ240121).

## 50 References

- [1] Olsen L C, Cabauy P and Elkind B J 2012 Betavoltaic power sources *Phys. Today* 65 (12) 35-38 <https://doi.org/10.1063/PT.3.1820>
- [2] Prelas M A, Boraas M, Aguilar F D, Seelig J D, Tchouaso M T and Wisniewski D 2016 In: *Nuclear Batteries and Radioisotopes (Lecture Notes in Energy* 56) (Springer Press, Switzerland)
- [3] Spencer M G and Alam T 2019 High power direct energy conversion by nuclear batteries *Appl. Phys. Rev.* 6 031305 <https://doi.org/10.1063/1.5123163>
- [4] Bower K, Barbanell Y, Shreter Y and Bohnert G 2002 In: *Polymers, Phosphors and Voltaics for Radioisotope Microbatteries* (CRC Press) pp. 352 <https://doi.org/10.1016/j.landurbplan.2010.08.017>
- [5] Wang H, Tang X B, Liu Y P, Xu Z H, Liu M and Chen D 2015 Temperature effect on betavoltaic microbatteries based on Si and GaAs under  $^{63}\text{Ni}$  and  $^{147}\text{Pm}$  irradiation *Nucl. Instrum. Methods Phys. Res. Sect. B* 359 36-43 <http://dx.doi.org/10.1016/j.nimb.2015.07.046>
- [6] Gui G, Zhang K, Blanchard J P and Ma Z Q 2016 Prediction of 4H-SiC betavoltaic micro battery characteristics based on practical Ni-63 sources *Appl. Radiat. Isot.* 107 272-277 <http://dx.doi.org/10.1016/j.apradiso.2015.11.001>
- [7] Cheng Z J, San H S, Li Y F and Chen X Y 2010 The design optimization for GaN-based betavoltaic microbattery In: 2010 IEEE 5th International Conference on Nano/Micro Engineered and Molecular Systems NEMS pp. 582-586 <https://doi.org/10.1109/NEMS.2010.5592469>
- [8] Cheng Z J, San H S, Chen X Y, Liu B and Feng Z H 2011 Demonstration of a high open-circuit voltage GaN betavoltaic microbattery *Chin. Phys. Lett.* 28 7 <https://doi.org/10.1088/0256-307X/28/7/078401>
- [9] Lu M, Zhang G G, Fu K, Yu G H, Su D and Hu J F 2011 Gallium nitride Schottky betavoltaic nuclear batteries *Energy Convers. Manag.* 52 (4) 1955-1958 <https://doi.org/10.1016/j.enconman.2010.10.048>
- [10] Liu Y M, Lu J B, Li X Y, Xu X, He R, Zheng R Z and Wei G D 2018 Theoretical prediction of diamond betavoltaic batteries performance using  $^{63}\text{Ni}$  *Chin. Phys. Lett.* 35 7 <https://doi.org/10.1088/0256-307X/35/7/072301>
- [11] Liu Y P, Tang X B, Xu Z H, Hong L, Wang H, Liu M and Chen D 2015 Influences of planar source thickness on betavoltaics with different semiconductors *J. Radioanal. Nucl. Chem.* 304 517-525 <https://doi.org/10.1007/s10967-014-3879-2>
- [12] Prelas M A, Weaver C L, Watermann M L, Lukosi E D, Schott R J and Wisniewski D A 2014 A review of nuclear batteries *Prog. Nucl. Energy* 75 117-148 <https://doi.org/10.1016/j.pnucene.2014.04.007>
- [13] Butera S, Lioliou G and Barnett A M 2017 Temperature effects on gallium arsenide  $^{63}\text{Ni}$

- 1 betavoltaic cell *Appl. Radiat. Isot.* 125 42-47  
2 http://dx.doi.org/10.1016/j.apradiso.2017.04.002
- 3 [14] YAKUBOVA G N 2010 *Nuclear batteries with*  
4 *tritium and promethium-147 radioactive*  
5 *sources*[D], Urbana: University of Illinois
- 6 [15] Chen H Y, Jiang L and Li D R 2011 Measurement  
7 of Beta Particles Induced Electron-Hole Pairs  
8 Recombination in Depletion Region of GaAs PN  
9 Junction *Chin. Phys. Lett.* 28 5 058101  
10 https://doi.org/10.1088/0256-307X/28/5/058101
- 11 [16] Chen H Y, Jiang L and Chen X Y 2011 Design  
12 optimization of GaAs betavoltaic batteries *J.*  
13 *Phys. D : Appl. Phys.* 44 215303  
14 https://doi.org/10.1002/er.4053
- 15 [17] Liu Y P, Tang X B, Ding D, Xie Q, Chen F D and  
16 Chen D 2012 Parameters optimization of GaAs  
17 betavoltaic microbattery *ATOMIC ENERGY*  
18 *SCI TECHNO* 46 Suppl
- 19 [18] Qiao D Y, Chen X J, Ren Y and Yuan W Z 2013 A  
20 micro nuclear battery based on SiC Schottky  
21 barrier diode *J. Microelectromech. Syst.* 20 (3)  
22 685-690  
23 https://doi.org/10.1109/JMEMS.2011.2127448
- 24 [19] San H S, Yao S L, Wang X, Cheng Z J and Chen X  
25 Y 2013 Design and simulation of GaN based  
26 Schottky betavoltaic nuclear micro-battery *Appl.*  
27 *Radiat. Isot.* 80 17-22  
28 https://doi.org/10.1016/j.apradiso.2013.05.010
- 29 [20] Neamen D A 2017 *Semiconductor Physics and*  
30 *Devices : Basic Principles*, 4th edn. (Publishing  
31 House of Electronics Industry, McGraw-Hill  
32 Education, Xi'an) pp. 248-630
- 33 [21] Blakemore J S 1982 Semiconducting and other  
34 major properties of gallium arsenide *J. Appl.*  
35 *Phys.* 53 R123 https://doi.org/10.1063/1.331665
- 36 [22] Adachi S 2005 In: *Properties of Group-IV, III-V*  
37  
38  
39  
40  
41  
42  
43  
44  
45  
46  
47  
48  
49  
50  
51  
52  
53  
54  
55  
56  
57  
58  
59  
60
- and II-VI Semiconductors (Wiley Series in Materials for Electronic & Optoelectronic Applications)
- [23] Wu M, Wang S M, Ou Y and Wang W B 2018 Optimization design of betavoltaic battery based on titanium tritide and silicon using Monte Carlo code *Appl. Radiat. Isot.* 142 22-27  
https://doi.org/10.1016/j.apradiso.2018.09.017
- [24] Klein C A 1968 Bandgap dependence and related features of radiation ionization energies in semiconductors *J. Appl. Phys.* 39 2029-2038  
https://doi.org/10.1063/1.1656484
- [25] Rahmani F and Khosravinia H 2016 Optimization of Silicon parameters as a betavoltaic battery: comparison of Si p-n and Ni/Si Schottky barrier *Radiat. Phys. Chem.* 125 205-212  
https://doi.org/10.1016/j.radphyschem.2016.04.012
- [26] Nejad G R, Rahmani F and Abaeiani G R 2014 Design and optimization of beta-cell temperature sensor based on  $^{63}\text{Ni}$ -Si *Appl. Radiat. Isot.* 86 46-51  
http://dx.doi.org/10.1016/j.apradiso.2013.12.027
- [27] Sze S and Ng M K 2007 *Physics of Semiconductor Devices*, 3rd ed. (John Wiley & Sons) pp. 720-727
- [28] Luque A and Hegedus A 2003 *Handbook of Photovoltaic Science and Engineering* (John Wiley, England) p. 91-92
- [29] Tang X B, Ding D, Liu Y P and Chen D 2012 Optimization design and analysis of Si- $^{63}\text{Ni}$  betavoltaic battery *Sci. China Technol. Sci.* 55 990-996  
https://doi.org/10.1007/s11431-012-4752-6